



Heterogeneous geometric designs in auxetic composites toward enhanced mechanical properties under various loading scenarios

Zhixiong Li ^a, Chengshuang Xie ^b, Feng Li ^a, Di Wu ^{b,c,*,**}, Nan Hu ^{a,d,*}

^a School of Civil Engineering and Transportation, South China University of Technology, Guangzhou, 510641, China

^b Guangdong Provincial Key Laboratory of Earthquake Engineering and Applied Technology, Guangzhou University, Guangzhou, 510006, China

^c Key Laboratory of Earthquake Resistance, Earthquake Mitigation and Structural Safety, Ministry of Education, Guangzhou, 510006, China

^d Pazhou Lab, Guangzhou, 510335, China



ARTICLE INFO

Keywords:

Composite design
Auxetics materials
Additive manufacturing
Complex loading
Energy dissipations

ABSTRACT

Cellular architected materials have demonstrated exceptional energy absorbing and dissipating capability mostly under compression, but integrating such geometric design strategy into a practical scenario requires consideration of a more complex loading state. In this study, we evaluate geometric patterns for 3D-printed core lattices embedded in silicone rubber composite units that are subjected to uniaxial compression, a combined compression-shear load, and loading-unloading cycles. Mechanical properties of composite units with regular cellular patterns were characterized under different loading scenarios through experiments and simulations. Our results show that various geometric patterns exhibit different advantages under certain loading conditions. Then, we further develop heterogeneous geometric patterns to achieve tailorably enhanced stiffness under compression and shear load. Finally, the developed composite units demonstrate excellent energy absorption under compressive loading-unloading cycles although slow stiffness degradations were observed. Our findings pave a way for integrating 3D printing into advanced composite designs for various energy-absorbing applications.

1. Introduction

Architected materials, a type of engineered materials with careful geometric designs, are known for unprecedented mechanical properties, such as negative Poisson's ratio, tunable stiffness, energy absorption, etc [1-5]. Previous studies have proved their great potential in a wide range of fields such as automotive, aerospace, construction, military, etc [6-9]. Coupled with emerging responsive materials and advanced geometric design, enhanced mechanical properties, and novel functions of architected materials including auxetic, lattice, and cellular materials have been investigated in the past few years [10-12]. To reach a higher level of strength and stiffness, composite materials embedded with architected geometric forms have been proposed [13-15], in which an auxetic core and a base material as a matrix are combined [16-19]. Extra efforts have been attempted by embedding various types of core materials in composite design [20-23], exploring different materials in the matrix phase [24-27], and integrating auxetic materials into structural designs

[28-30]. Thanks to recent advances in additive manufacturing, the freedom of material selections and the versatility of geometric designs of the auxetic cores have been further enabled [31-33]. Despite all these efforts, most studies have only considered a single loading scenario including compression, tension, indentation, pure shear, or dynamic impact [34-37]. However, composite materials are most likely subjected to dual or combined loadings in practice, which motivated us to search for advanced geometric patterns and their spatial arrangement that can satisfy various loading scenarios.

In this work, we investigated the behavior of soft architected composite (SAC) units embedded with various 3D-printed cores that were fabricated by a common additive manufacturing approach (i.e. FDM printing) through a commercial printer in our research lab. We evaluated three types of SAC units embedded with re-entrant cores (negative Poisson's ratio), honeycomb cores (positive Poisson's ratio), and hybrid cores combining two prior patterns. Guided by experimental tests and numerical simulations, we compared the deformation modes and

* Corresponding author. School of Civil Engineering and Transportation, South China University of Technology, Guangzhou, 510641, China.

** Corresponding author. Guangdong Provincial Key Laboratory of Earthquake Engineering and Applied Technology, Guangzhou University, Guangzhou, 510006, China.

E-mail addresses: 11795234@qq.com (D. Wu), nahu026@scut.edu.cn (N. Hu).

mechanical responses of those SAC units under compression and compression-shear loadings. According to the obtained geometric principles, several heterogeneous core geometries were proposed for SAC units and their performances were evaluated. Finally, we explored the performance of the SAC units under compressive loading-unloading cycles to ensure their feasibility in engineering applications.

2. Material and methods

2.1. Fabrication, mechanical tests and simulations

The 2D core lattices of SAC units were made of Polylactic Acid (PLA) and fabricated by the Fused Deposition Modelling (FDM) method through a commercial 3D printer Laseradd-i2c. We selected PLA instead of other printing materials because it is high spiffiness, high ductility, and recyclable. Specific printing parameters include the printing speed of 80 mm/s, nozzle temperature of 215 °C, layer height of 0.25 mm, which was applied to all lattice specimens. The soft matrix adopts silicone rubber as the base material. The fabrication process of SAC units was carried out in three stages as given in Fig. 1a. First, the core lattices were placed in a 3D-printed casting mold in which their inner surface is coated with wax for a better mold release later. Then, we slowly poured the liquid silicone rubber mixture into the casting setup. The compactness of the mixture was checked to avoid hollow areas between core lattices and casting molds. We smoothed the open end of the mold where the extra mixture was left after the pouring process before keeping them at room temperature for 24 h. After the mixture was solidified, we eventually removed SAC units from the mold and measured their dimension before each experimental series. A total of 31 SAC units were made using the same procedure (see Table S1 in the Supplementary data).

We performed experimental tests on SAC units and evaluated their mechanical behaviors subjected to various loading scenarios (Fig. 1b).

The uniaxial compression tests were performed under displacement control with a speed of 0.04 mm/s using a universal mechanical testing machine (GRANDTRY TESTER, Guangzhou, 100 kN load cell). The shear performance of SAC units was tested using the compression shear testing machine (DAJ-100, Changchun, 30 KN cell). The SAC units were firstly compressed under a constant vertical load of about 5 kN and then pushed laterally in displacement-controlled loading consisting of cycles for 4 mm and 6 mm at a rate of 0.05 Hz. The cyclic load tests were conducted on the same machine for the axial compressive test yet subjected to four cycles with the same displacement and multiple cycles with incremental displacement. Details of the experimental setups mentioned here can be found in Fig. S1. The numerical simulations were performed using the commercial finite element (FE) package ABAQUS/Standard (see Figs. S2–S4).

2.2. Design of core geometries and finite element analysis

The unit cell of the core geometry adopted in this study is shown in Fig. 1a, which is designed based on Gibson's model [38], where the parameters are described by equations: $\theta = \arctan(v_l/h)$, $B = (h - l \tan \theta)/2$, $D = l/(2 \cos \theta)$. Here, we fix the overall dimension of the unit cell with the parameters of $h = l = 10$ mm, and vary the value of Poisson's ratio (v_c) to generate core geometries by periodically arranging cells (see Fig. S5). We chose the lower-bound design of the re-entrant unit cell ($v_c = -0.6$) and the upper-bound design of the honeycomb unit cell ($v_c = 0.6$) as shown in Fig. 1c. We selected sideways re-entrant pattern because the transverse re-entrant pattern cannot be combined with honeycomb pattern although the auxetic effect may lose partially. To design a SAC unit, we arrange a total of 32 (4 × 8) unit cells of each core pattern, resulting in the overall dimension with a height of $H = 40$ mm, a width $L = 80$ mm, and a depth of $T = 70$ mm. SAC units with re-entrant cores (negative v_c) and honeycomb cores (positive v_c) were primarily investigated and later hybrid cores combining two basic patterns

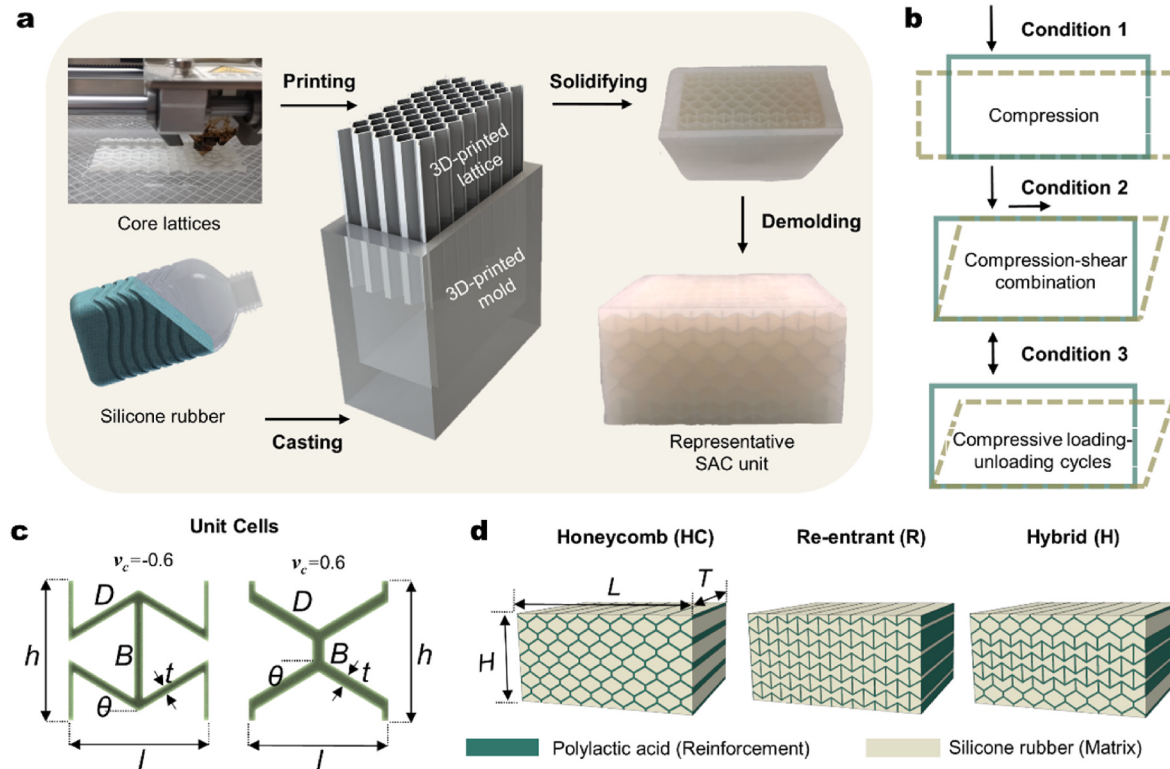


Fig. 1. Fabrication and design of soft architected composite (SAC) units. (a) The fabrication process. (b) The loading conditions in this study. (c) The geometric parameters of the re-entrant and the honeycomb unit cell. h and l are the height and length of the unit cell; B is the length of the vertical strut and D is the length of the inclined strut; t is the thickness of the strut; θ represents the inclination angle. (d) Three SAC units with different 3D-printed cores.

were proposed, as shown in Fig. 1d. The volume fraction (V_c) of the core lattice in a SAC unit is controlled to 20% (in the first series) and 30% (in the second series) by tailoring the strut thickness in each core geometries.

3. Results and discussions

3.1. Compressive and compressive-shear behaviors of the SAC units

We first compared the mechanical behavior of three SAC units with honeycomb (HC), re-entrant (R), and hybrid (H) cores along with the response of a baselined silicone rubber unit under uniaxial compressive loading (Fig. 2). In this loading condition, we define a dimensionless ratio of δ_1/H to describe a generalized axial displacement where δ_1 represent the actual axial displacement and H is the total height of the SAC unit (i.e. 40 mm). Fig. 2a summarizes the simulated and experimental deformations for all SAC units in which all of them were shortened by 4 mm (i.e., $\delta_1/H = 0.1$). At the $\delta_1/H = 0.1$, the SAC-R unit experienced a sideway buckling but the SAC-H unit exhibited an auxetic effect in terms of lateral contraction. We also observed significant extrusion of rubber on the front and back of the SAC units due to the constraint of the lattice core (see Fig. S6). Responses of two other hybrid patterns were evaluated by switching re-entrant and honeycomb cells at different rows (Fig. S7) and found that deformation modes are similar to either the SAC-R unit or the SAC-HC unit depending on which geometry is placed on the middle portion. Nevertheless, simulations and experiments showed agreement in terms of qualitative behavior. The variations of Poisson's ratio (v_c) versus the dimensionless ratio of δ_1/H obtained by numerical simulations were plotted in Fig. 2b. The value of v_c is estimated by calculating the lateral strain of the mid-height plane over the axial strain from the numerical model. It can be seen that v_c of

the rubber unit and the SAC-HC unit stayed at a positive value and slightly varied between 0.5 and 0.6. v_c of the SAC-R unit stays negative when δ_1/H is below 0.03 but experiences a dramatic increase of v_c at large strain, accompanied by the occurrence of localized buckling of struts that are caused by stress concentration. For the SAC-H unit, the v_c value is slightly below zero before δ_1/H is smaller than 0.06 and then gradually increases.

To compare compressive response among SAC units, the dimensionless force-displacement curves are plotted in Fig. 2c. The non-dimensional force is defined by the ratio of actual load (F_1) over $E \times T \times L$ (E denoting the elasticity modulus of PLA). It can be seen the SAC-R unit has the largest stiffness before reaching the peak load. Specifically, we calculated the secant stiffness K_1 from the linear portion (δ_1/H from 0.02 to 0.04) of the response curve under axial compression and found that the K_1 value of the SAC-R unit (33.28×10^3) is eight times higher than that of the SAC-HC unit (4.8×10^3). Several load drops were observed in its response curve after the peak point because the fracture occurred in the core lattice during the loading process which eventually resulted in broken struts inside the unit. Our simulated results are consistent with the experimental results in terms of initial stiffness but the numerical model does not capture the broken lattice inside the unit under large deformation, thus no "drops" are found in the simulations. Meanwhile, a typical densification response in lattice alone disappeared in the SAC units. Overall, the SAC-R unit with a v_c value exhibits an enhanced compressive behavior yet the SAC-H unit shows a controlled deformation and tunable behavior due to hybrid patterns. The compressive strength of all three SAC units is significantly higher than that of the rubber unit due to the presence of the core lattice.

After evaluating the mechanical behavior of SAC units under uniaxial compression, we explored their behaviors under combined compression-shear load. These units were axially compressed under the

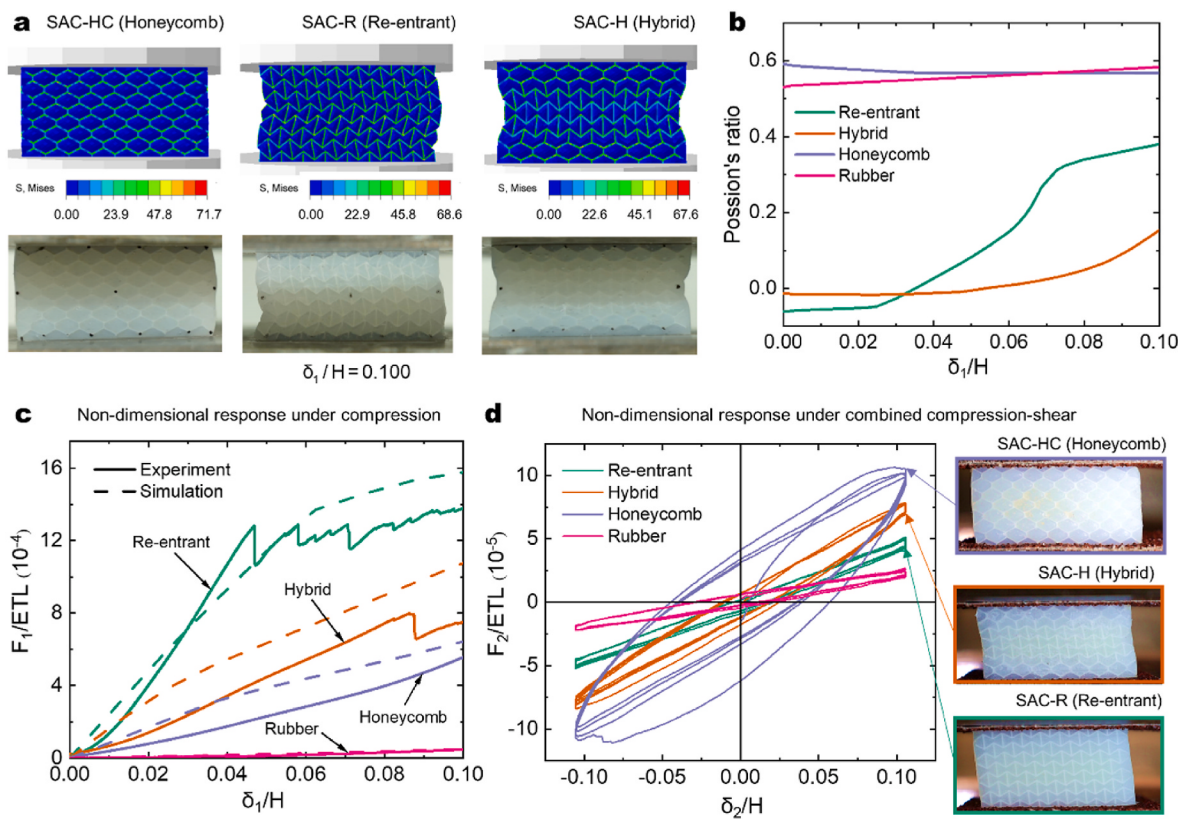


Fig. 2. Mechanical response of SAC units and silicone rubber unit under uniaxial compressive loading. (a) Simulated von Mises stress contours and experimental deformation process at various dimensionless compressive strain levels for each unit. (b) Numerically simulated variation of the Poisson's ratios (v_c) for three SAC units and the rubber unit. (c) Numerical and experimental dimensionless force-displacement curves for SAC units and the rubber unit. (d) The non-dimensional hysteretic curves for three SAC units under combined compression-shear loading.

identical load (5 kN) and then were pushed horizontally. We defined two non-dimensional parameters F_2/ETL to describe lateral shear force and δ_2/H to measure the lateral displacement. We also calculated the secant stiffness K_2 using a portion of a response curve (δ_2/H from -0.1 to 0.1). In Fig. 2d, we compared the dimensionless force-displacement hysteretic curves of three SAC units and found that the influence of the core patterns on the compressive-shear behavior shows an opposite trend to the compressive behavior. The SAC-HC unit has the lowest K_1 under compression but has the highest K_2 value (10.14×10^{-4}) and the largest enclosed area of the total hysteretic curve (3.03×10^{-5}) among the three SAC units. In contrast, the SAC-R unit has the weakest K_2 (5.36×10^{-4} , half of the SAC-HC unit) and the smallest enclosed area (0.44×10^{-5} , only 1/7 of the SAC-HC unit), because the struts of the re-entrant lattice perform better in bending than stretching. In between, SAC-H units can numerous K_1-K_2 combination, which can be tuned by geometric designs. Fig. 2d also compares the deformations among three SAC units in which the SAC-R unit has the largest shear angle. Experimental and numerical hysteretic curves and the deformation process for the SAC-H unit are presented in Figs. S8 and S9. The magnitude of axial load levels also plays a role in the hysteretic response of SAC-H units (Fig. S10). Overall, our results show that various geometric patterns exhibit different advantages under certain loading conditions.

3.2. Design and analysis of SAC units with novel heterogeneous core patterns

We further develop heterogeneous geometric patterns by combining several basic unit cells discussed above for enhanced mechanical behavior as shown in Fig. 3a. Instead of layered patterns, we combined the truss pattern with the re-entrant pattern and the honeycomb pattern to form the SAC-RT unit and the SAC-HCT unit, respectively. These two units stayed with the same overall dimension but the size of the unit cell was increased from 10×10 mm to 20×20 mm to satisfy the limit on shell thickness of the 3D printer, leading to a 4×2 arrangement and the volume fraction of 30%. To compare their performance with SAC units

using single lattice patterns, we also fabricated three SAC units with re-entrant, rectangle, and honeycomb cores. The non-dimensional force-displacement responses of SAC units under compression were obtained experimentally as given in Fig. 3b. Again, the compressive stiffness of SAC units with regular core patterns decreases as the Poisson's ratio of a given unit increases, in which the SAC unit with the re-entrant pattern ($v_c = -0.4$) has the largest compressive stiffness among three units. It is interesting to see that under the same volume fraction (i.e. same weight) of core lattice the compressive stiffness values of the SAC-RT unit and the SAC-HCT unit are 38% and 53.5% higher than that of SAC units with regular re-entrant and honeycomb patterns, respectively, due to the introduction of truss pattern. In particular, the truss pattern provided additional load paths to the re-entrant pattern where stress concentrations were less significant, resulting in the largest compressive stiffness in the SAC-RT unit.

In Fig. 3c, the shear behaviors of five SAC units through numerical simulations are found. Among them, the results of three SAC units with regular lattice cores are consistent with the observations in Fig. 2d. The SAC-HC unit has the highest shear stiffness K_2 and the SAC-R unit has the lowest shear stiffness among the three regular SAC units. The advantage of using heterogeneous patterns in the SAC-RT unit and the SAC-HCT unit lead to 475% and 66.7% higher in K_2 values than that of SAC units with regular re-entrant and honeycomb patterns. For the SAC-HCT unit, the truss structure protects the vertical wall from buckling and distributes stress more rationally such that the enhanced shear behavior is achieved (see Fig. S11 for the detailed stress distribution). The non-dimensional energy absorptions of five SAC units under two loading scenarios were calculated to confirm the advantage of using the heterogeneous patterns as shown in Fig. 3d. Apparently, the SAC-RT unit and the SAC-HCT unit led compressive and shear loading scenario, respectively, showing enhanced energy absorptions in each category. Overall, the SAC unit can be further tailored by introducing novel geometric patterns on the core lattice.

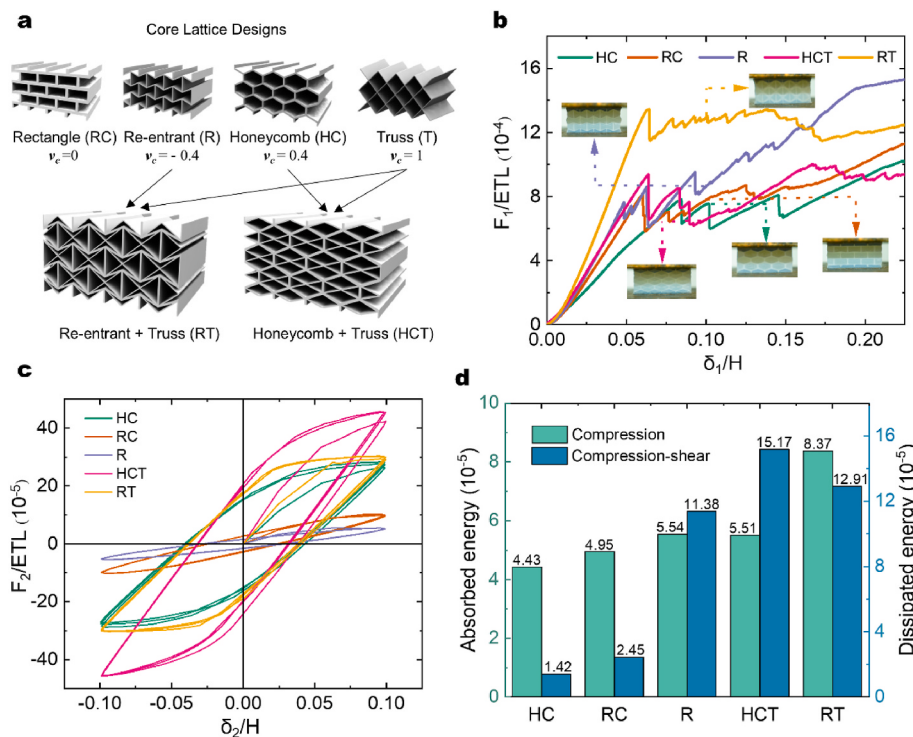


Fig. 3. Design and mechanical response of SAC units embedded with heterogeneous patterns. (a) formation of heterogeneous patterns. (b) The obtained mechanical response of SAC units under axial compression. (c) The nondimensional force-displacement response of SAC units under shear loading cycles through numerical simulations. (d) Energy absorption and dissipation of SAC units with different core patterns under compressive and compressive-shear load, respectively.

3.3. Mechanical behavior of SAC units under compressive loading-unloading cycles

From the experimental results above, we found that the stiffnesses of SAC units are weakened under large displacement but we assume that the broken core lattice inside the unit may still play a role, which motivated us to repeat compression tests to evaluate their post-damage behavior. Fig. 4a presents the response curves of the SAC-R unit under three loading-unloading cycles till the same axial displacement ($\delta_1/H = 0.225$). The stiffness of the SAC-R unit is significantly reduced in the second and the third cycle due to the severe fracture of the lattice in the first cycle. The SAC-R unit maintained a higher load-carry capacity and stiffness compared to the rubber unit. Distinguished by their volume fraction ratio (20% and 30%), seven other SAC units also demonstrated the same response feature (see Figs. S12–S14). Fig. 4b compares the total absorbed energy (sum of three load cycles below the response curve till $\delta_1/H = 0.1$) of all SAC units from two testing groups in which the SAC-R unit and the SAC-RT unit have the highest absorbed energy in each group. In the second group with a volume fraction ratio of 30%, the absorbed energy of the SAC-RT unit is only 9.57% higher than the SAC-R unit due to severe damage in the core lattice after the first load cycle.

To mitigate the effect of material fracture on the following cycles, we further fabricated a new testing series of SAC units and incrementally compressed them for nine loading-unloading cycles with an interval of 1 mm ($\delta_1/H = 0.025$). Fig. 4c shows the hysteretic curve of nine cycles for the SAC-R unit. The SAC-R unit maintained the elastic response for two cycles (δ_1/H from 0 to 0.05) and started to exhibit load drops in the loading phase of the third cycle, indicating localized failure of the core lattice. Starting in the fourth load cycle, gradual stiffness degradations were observed due to the pre-existed damage but the SAC-R unit still exhibited an incremental increase in peak load and energy absorption capability till the end of the ninth cycle. In Fig. 4d, we compared the total dissipated energy of all SAC units under nine cycles. Similar to the previous series, the SAC-R unit and the SAC-RT unit with a 20% volume fraction have the largest dissipated energy among each group. In the second group with a 30% volume fraction, the dissipated energy values

of the SAC-HCT unit and the SAC-RT unit are 114% and 62% higher than their corresponding SAC units with the single lattice pattern. Overall, our experiments confirmed that the core lattices can maintain their reinforcing roles under load cycles and still contribute to the performance of SAC units after damage.

4. Conclusions

In summary, we investigated a soft architected composite (SAC) by embedding various 3D-printed cellular patterns into a soft matrix. Guided by experiments and simulations, we found that (1) by adding an appropriate lattice pattern in the soft matrix, the SAC unit can achieve enhanced performance under different loading scenarios. Specifically, the best performers in each scenario are the re-entrant pattern for compression and cyclic load, and the honeycomb pattern for shear loading. (2) SAC units with hybrid and heterogeneous patterns offered additional response tunability, controlled failure modes, and enhanced mechanical properties under all loading scenarios compared to SAC units with single patterns under the same volume fraction ratio. (3) It is interesting to find that the core lattice can maintain its strength and stiffness under multiple loading-unloading cycles and meanwhile still contribute to the performance of SAC units after damage. The geometric principle learned in this study can be applied to composite material design in various scales. Despite these findings, continuing efforts can be made on several fronts: (1) the effect of additive manufacturing parameters on the performance of SAC units is not clear. (2) the effect of diverse geometric patterns (3D lattice, non-uniformed, etc.) should be investigated through advanced digital approaches such as machine learning, topology optimization, etc. (3) Performance targets should be well defined depending on a specific application scenario such that an inverse approach can be applied to design appropriate dimension, select suitable materials, and identify geometric patterns. Overall, we envision that our study can pave the way for integrating 3D-printed constituents into developing advanced composite materials and structures with enhanced performance at various length scales such as protection devices, elastic joints, bearings, etc.

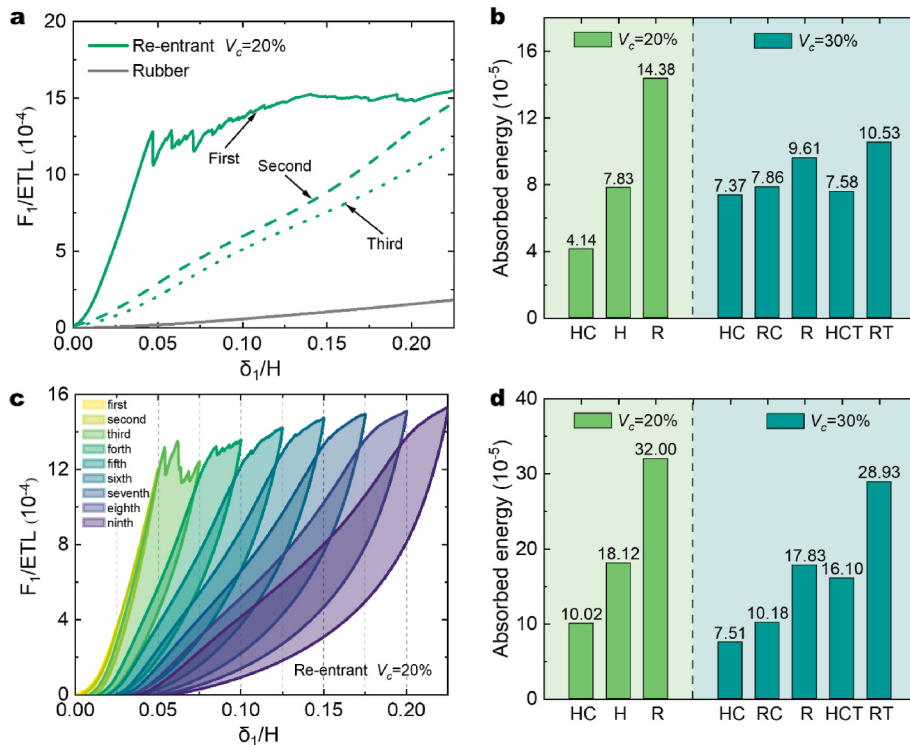


Fig. 4. Mechanical response of the SAC units and silicone rubber under cyclic compressive loading.

(a) The nominalized force-displacement response of the SAC-R unit ($V_c = 20\%$) under three repeated loading till $\delta_1/H = 0.225$. (b) Total energy absorption of all SAC units under three repeated compressive loading. (c) The nominalized force-displacement response of the SAC-R unit ($V_c = 20\%$) under nine loading-unloading cycles with an interval of 0.025 mm for each cycle. (d) Total energy dissipation of SAC units under nine loading-unloading cycles.

CRediT authorship contribution statement

Zhixiong Li: Data curation, Investigation, Methodology, Validation, Writing – original draft. **Chengshuang Xie:** Investigation. **Feng Li:** Investigation. **Di Wu:** Conceptualization, Funding acquisition, Supervision, Writing – review & editing. **Nan Hu:** Conceptualization, Funding acquisition, Methodology, Project administration, Resources, Supervision, Writing – original draft, Writing – review & editing.

Declaration of competing interest

The authors declare that they have no known competing financial interests or personal relationships that could have appeared to influence the work reported in this paper.

Data availability

Data will be made available on request.

Acknowledgments

This work was financially supported by the National Natural Science Foundation of China (52008174 and 52178281), and Guangdong Provincial Key Laboratory of Modern Civil Engineering Technology (2021B1212040003).

Appendix A. Supplementary data

Supplementary data to this article can be found online at <https://doi.org/10.1016/j.coco.2023.101499>.

References

- [1] C. Luo, C.Z. Han, X.Y. Zhang, X.G. Zhang, X. Ren, Y.M. Xie, Design, manufacturing and applications of auxetic tubular structures: a review, *Thin-Walled Struct.* 163 (2021), 107682.
- [2] I.P. Seethoh, X. Liu, K. Markandan, L. Zhen, C.Q. Lai, Strength and energy absorption characteristics of Ti6Al4V auxetic 3D anti-tetrachiral metamaterials, *Mech. Mater.* 156 (2021), 103811.
- [3] Z. Li, K. Wang, B. Wang, Indentation resistance of brittle auxetic structures: combining discrete representation and continuum model, *Eng. Fract. Mech.* 252 (2021), 107824.
- [4] J. Liu, W. Chen, H. Hao, Z. Wang, In-plane crushing behaviors of hexagonal honeycombs with different Poisson's ratio induced by topological diversity, *Thin-Walled Struct.* 159 (2021).
- [5] M.-S. Pham, C. Liu, I. Todd, J. Lerthanasarn, Damage-tolerant architected materials inspired by crystal microstructure, *Nature* 565 (7739) (2019) 305–311.
- [6] Y. Zhang, X. Ren, X.Y. Zhang, T.T. Huang, L. Sun, Y.M. Xie, A novel buckling-restrained brace with auxetic perforated core: experimental and numerical studies, *Eng. Struct.* 249 (2021).
- [7] R.P. Bohara, S. Linforth, A. Ghazlan, T. Nguyen, A. Remennikov, T. Ngo, Performance of an auxetic honeycomb-core sandwich panel under close-in and far-field detonations of high explosive, *Compos. Struct.* 280 (2022), 114907.
- [8] H. Tan, Z. He, E. Li, A. Cheng, T. Chen, X. Tan, Q. Li, B. Xu, Crashworthiness design and multi-objective optimization of a novel auxetic hierarchical honeycomb crash box, *Struct. Multidiscip. Optim.* 64 (4) (2021) 2009–2024.
- [9] C. Qi, F. Jiang, S. Yang, A. Remennikov, S. Chen, C. Ding, Dynamic crushing response of novel re-entrant circular auxetic honeycombs: numerical simulation and theoretical analysis, *Aero. Sci. Technol.* 124 (2022), 107548.
- [10] X. Xia, C.M. Spadaccini, J.R. Greer, Responsive materials architected in space and time, *Nat. Rev. Mater.* (2022) 1–19.
- [11] M. Kadic, G.W. Milton, M. van Hecke, M. Wegener, 3D metamaterials, *Nat. Rev. Phys.* 1 (3) (2019) 198–210.
- [12] M. Benedetti, A. Du Plessis, R. Ritchie, M. Dallago, S. Razavi, F. Berto, Architected cellular materials: a review on their mechanical properties towards fatigue-tolerant design and fabrication, *Mater. Sci. Eng. R Rep.* 144 (2021), 100606.
- [13] Z. Wang, Recent advances in novel metallic honeycomb structure, *Compos. B Eng.* 166 (2019) 731–741.
- [14] R. Zhong, X. Ren, X.Y. Zhang, C. Luo, Y. Zhang, Y.M. Xie, Mechanical properties of concrete composites with auxetic single and layered honeycomb structures, *Construct. Build. Mater.* 322 (2022), 126453.
- [15] X.-L. Peng, C. Soysal, S. Bargmann, Phase contrast mediated switch of auxetic mechanism in composites of infilled re-entrant honeycomb microstructures, *Extreme Mech. Lett.* 35 (2020), 100641.
- [16] J.-X. Wang, X. Liu, Q.-S. Yang, R. Tao, Y. Li, L.-H. Ma, A novel programmable composite metamaterial with tunable Poisson's ratio and bandgap based on multi-stable switching, *Compos. Sci. Technol.* 219 (2022), 109245.
- [17] R. Johnston, Z. Kazanci, Analysis of additively manufactured (3D printed) dual-material auxetic structures under compression, *Addit. Manuf.* 38 (2021), 101783.
- [18] W. Guo, Y. Huang, R.O. Ritchie, S. Yin, Dissipative dual-phase mechanical metamaterial composites via architectural design, *Extreme Mech. Lett.* 48 (2021), 101442.
- [19] D. Yavas, Q. Liu, Z. Zhang, D. Wu, Design and fabrication of architected multi-material lattices with tunable stiffness, strength, and energy absorption, *Mater. Des.* 217 (2022), 110613.
- [20] M.M. Osman, M. Shazly, E.A. El-Danaf, P. Jamshidi, M.M. Attallah, Compressive behavior of stretched and composite microlattice metamaterial for energy absorption applications, *Compos. B Eng.* 184 (2020), 107715.
- [21] N. Novak, L. Krstulović-Opara, Z. Ren, M. Vesenjak, Mechanical properties of hybrid metamaterial with auxetic chiral cellular structure and silicon filler, *Compos. Struct.* 234 (2020), 111718.
- [22] Z. Jia, Z. Deng, L. Li, Biominerilized materials as model systems for structural composites: 3D architecture, *Adv. Mater.* (2022), 2106259.
- [23] Z. Zhang, H. Zhu, R. Yuan, S. Wang, T. Fan, Y. Rezgui, D. Zhang, The near-isotropic elastic properties of interpenetrating composites reinforced by regular fibre-networks, *Mater. Des.* (2022), 110923.
- [24] T. Fila, P. Zlámal, O. Jiroušek, J. Falta, P. Koudelka, D. Kytyřík, T. Doktor, J. Valach, Impact testing of polymer-filled auxetics using split Hopkinson pressure bar, *Adv. Eng. Mater.* 19 (10) (2017), 1700076.
- [25] Y. Xue, W. Wang, F. Han, Enhanced compressive mechanical properties of aluminum based auxetic lattice structures filled with polymers, *Compos. B Eng.* 171 (2019) 183–191.
- [26] Y. Xue, J. Mu, Y. Huang, L. Zhou, Z. Shi, Compressive mechanical properties of ex-situ auxetic composite-filled tubes, *J. Mater. Res. Technol.* 14 (2021) 1644–1654.
- [27] W. Xu, P. Ma, L. Wu, G. Jiang, Low-velocity impact properties of composite reinforced by auxetic warp-knitted spacer fabric, *J. Sandw. Struct. Mater.* 23 (6) (2021) 1972–1986.
- [28] H. Gu, A.D. Shaw, M. Amoozgar, J. Zhang, C. Wang, M.I. Friswell, Twist morphing of a composite rotor blade using a novel metamaterial, *Compos. Struct.* 254 (2020), 112855.
- [29] C. Li, H.-S. Shen, J. Yang, Multi-scale modeling and numerical analysis of sandwich beams with FG auxetic 3D lattice cores and GRC face sheets subjected to drop-weight impacts, *Eng. Struct.* 265 (2022), 114486.
- [30] F. Usta, H.S. Türkmen, F. Scarpa, Low-velocity impact resistance of composite sandwich panels with various types of auxetic and non-auxetic core structures, *Thin-Walled Struct.* 163 (2021), 107738.
- [31] F. Albertini, J. Dirrenberger, C. Sollogoub, T. Maconachie, M. Leary, A. Molotnikov, Experimental and computational analysis of the mechanical properties of composite auxetic lattice structures, *Addit. Manuf.* 47 (2021), 102351.
- [32] Y. Zhang, M.-T. Hsieh, L. Valdevit, Mechanical performance of 3D printed interpenetrating phase composites with spinodal topologies, *Compos. Struct.* 263 (2021), 113693.
- [33] T. Li, Y. Chen, X. Hu, Y. Li, L. Wang, Exploiting negative Poisson's ratio to design 3D-printed composites with enhanced mechanical properties, *Mater. Des.* 142 (2018) 247–258.
- [34] H. Zhou, K. Jia, X. Wang, M.-X. Xiong, Y. Wang, Experimental and numerical investigation of low velocity impact response of foam concrete filled auxetic honeycombs, *Thin-Walled Struct.* 154 (2020), 106898.
- [35] M. Shaat, A.R. El Dhaba, On the equivalent shear modulus of composite metamaterials, *Compos. B Eng.* 172 (2019) 506–515.
- [36] T. Okumura, R. Takahashi, K. Hagita, D.R. King, J.P. Gong, Improving the strength and toughness of macroscale double networks by exploiting Poisson's ratio mismatch, *Sci. Rep.* 11 (1) (2021) 1–13.
- [37] T. Li, F. Liu, L. Wang, Enhancing indentation and impact resistance in auxetic composite materials, *Compos. B Eng.* 198 (2020), 108229.
- [38] L. Gibson, M. Ashby, *Cellular Solids: Structure and Properties*, Cambridge Univ. Pr, 1999.